

The Formation of Cr-Al Spinel under a Reductive Atmosphere

Oleksandr Shtyka , Waldemar Maniukiewicz , Radosław Ciesielski , Adam Kedziora, Viktor Shatsila , Tomasz Sierański  and Tomasz Maniecki 

Institute of General and Ecological Chemistry, Lodz University of Technology, 90924 Lodz, Poland; waldemar.maniukiewicz@p.lodz.pl (W.M.); radoslaw.ciesielski@p.lodz.pl (R.C.); adam.kedziora@p.lodz.pl (A.K.); viktar.shatsila@dokt.p.lodz.pl (V.S.); tomasz.sieranski@p.lodz.pl (T.S.); tomasz.maniecki@p.lodz.pl (T.M.)

* Correspondence: oleksandr.shtyka@p.lodz.pl

Abstract: In the present work, for the first time, the possibility of formation of CrAl_2O_4 was shown from the equimolar mixture of co-precipitated Al_2O_3 and Cr_2O_3 oxides under a reductive environment. The crystallographic properties of the formed compound were calculated using the DICVOL procedure. It was determined that it has a cubic crystal structure with space group $\text{Fd-}3\text{m}$ and a unit cell parameter equal to $8.22(3) \text{ \AA}$. The formed CrAl_2O_4 is not stable under ambient conditions and easily undergoes oxidation to $\alpha\text{-Al}_2\text{O}_3$ and $\alpha\text{-Cr}_2\text{O}_3$. The overall sequence of the phase transformations of co-precipitated oxides leading to the formation of spinel structure is proposed.

Keywords: Al_2O_3 ; Cr_2O_3 ; Cr; CrAlO_3 ; spinel; reduction process



Citation: Shtyka, O.; Maniukiewicz, W.; Ciesielski, R.; Kedziora, A.; Shatsila, V.; Sierański, T.; Maniecki, T. The Formation of Cr-Al Spinel under a Reductive Atmosphere. *Materials* **2021**, *14*, 3218. <https://doi.org/10.3390/ma14123218>

Academic Editors: Alain Largeteau and Sotirios Christodoulou

Received: 28 April 2021

Accepted: 7 June 2021

Published: 10 June 2021

Publisher's Note: MDPI stays neutral with regard to jurisdictional claims in published maps and institutional affiliations.



Copyright: © 2021 by the authors. Licensee MDPI, Basel, Switzerland. This article is an open access article distributed under the terms and conditions of the Creative Commons Attribution (CC BY) license (<https://creativecommons.org/licenses/by/4.0/>).

1. Introduction

Aluminum oxide is an important inorganic compound that is extensively used in many industrial applications. It is also an important mineral (e.g., corundum) and a precious gemstone (e.g., ruby and sapphire). It has many crystalline polymorphic phases such as $\alpha\text{-Al}_2\text{O}_3$, $\gamma\text{-Al}_2\text{O}_3$, $\delta\text{-Al}_2\text{O}_3$, $\theta\text{-Al}_2\text{O}_3$, $\eta\text{-Al}_2\text{O}_3$, $\kappa\text{-Al}_2\text{O}_3$, $\chi\text{-Al}_2\text{O}_3$, and $\rho\text{-Al}_2\text{O}_3$ [1]. Among them, $\alpha\text{-Al}_2\text{O}_3$ is the most stable alumina phase. The corundum structure consists essentially of a dense arrangement of oxygen ions in hexagonal closest packing with Al^{3+} ions occupying two-thirds of the available octahedrally coordinated sites.

Due to its structure, $\alpha\text{-Al}_2\text{O}_3$ has some valuable physical and chemical properties such as good acid, alkali, and heat resistances; and high hardness and strength. It is widely used in different fields such as ceramics, surface protective layer materials, refractory materials, and optical materials [2].

Another commonly used form of alumina is $\gamma\text{-Al}_2\text{O}_3$. Its structure can be regarded as spinel type in which oxygen atoms are arranged in a cubic close packing and Al atoms occupy the octahedrally and tetrahedrally coordinated sites. $\gamma\text{-Al}_2\text{O}_3$, which is also called activated alumina, has a large surface area and strong adsorption capacity, and therefore is widely employed as absorbents, catalyst supports, chromatographic media, and ion exchanges [3–5].

Aluminum oxides are usually obtained via the heat treatment of aluminum hydroxides, e.g., boehmite or aluminum salts. The formation of one or another form of alumina depends mainly on the type and properties of the starting material and conditions of the process. In general, all of the transition aluminas transfer into the other modifications at about $600 \text{ }^\circ\text{C}$ and all are transformed into the thermally stable $\alpha\text{-Al}_2\text{O}_3$ at temperatures above $1000 \text{ }^\circ\text{C}$ [6].

The physicochemical properties of Al_2O_3 can be considerably altered by incorporation of second phase particles such as ZrO_2 , SiC , SnO_2 , B_4C , TiC , Cr_3C_2 , and Cr_2O_3 [7–10]. Such modifications were reported to be beneficial for improving the mechanical properties of Al_2O_3 -based ceramics [11,12]. Moreover, it was reported that the catalysts supported on Al_2O_3 -based binary systems are superior in comparison with those supported on Al_2O_3 alone [13].

An interesting approach to modifying the properties of Al_2O_3 is the incorporation of Cr_2O_3 into its structure. Corundum (Al_2O_3) and eskolaite (Cr_2O_3) are isostructural, and Al^{3+} and Cr^{3+} ions have similar ionic radii. For this reason, they have similar unit cell parameters with a mismatch of ~4% [14]. Therefore, at high temperatures, Cr_2O_3 may form a substitutional solid solution in an Al_2O_3 lattice by exchange with Al^{3+} ions over the full range of compositions without formation of any eutectic. Depending on the content of Cr_2O_3 or Al_2O_3 , these solutions can be divided into corundum and eskolaite by the dominant-constituent rule [15]. These materials are used as refractory materials as well as in several other applications [16].

The process of formation of substitutional solid solutions is energy-intensive and requires high temperatures at which the formation of spinel structure compounds can also occur. For instance, Sako [17] and Ping [18] reported the formation of MgAl_2O_4 from the corresponding oxides at temperatures as high as 1000 °C. The ordinary spinel structure, with a general formula of AB_2O_4 (where A^{2+} and B^{3+} are usually metal ions), is related to the arrangement of the octahedra that are the main framework of the spinel structure. This can explain relatively high hardness and high density usually observed for this group of compounds. In the normal spinel structure, the O^{2-} ions form a face-centered cubic array with A^{2+} and B^{3+} cations occupying one-eighth of the tetrahedrally and one-half of the octahedrally coordinated sites, respectively. In an inverse spinel $\text{B}(\text{AB})\text{O}_4$, alternatively, one-eighth of the tetrahedrally coordinated sites are occupied by cation B^{3+} whereas A^{2+} and B^{3+} each occupy one-quarter of the octahedrally coordinated sites. Usually, spinel compounds crystallize in the high symmetry space group type $Fd-3m$, but lower symmetries also occur [19]. The mechanism of formation of spinel compounds was investigated by many researchers, particularly Rossi [20], Carter [21], and Navias [22], who performed mechanistic studies related to the formation of magnesium aluminate spinel. Their results showed that the reaction proceeds through interdiffusion of Al^{3+} and Mg^{2+} ions through the oxygen array. Particularly, Al^{3+} ions migrate from the alumina particles to the magnesia ones and Mg^{2+} diffuses in the opposite direction, leading to the spinel layer formation at the interface between the alumina and magnesia particles.

The aim of the current research work was to investigate the possibility of the formation of a spinel structure from the aluminum and chromium oxides. It was assumed that under conditions of high temperature and a reductive atmosphere the formation of Cr^{2+} ions may occur, which would further diffuse into an Al_2O_3 matrix.

Moreover, we attempted to investigate the phase transformation of both aluminum and chromium oxides and the interaction between them as a function of temperature.

2. Experimental

2.1. Preparation of Samples

The mixture of aluminum and chromium oxides was prepared by a co-precipitation method using water solutions of corresponding nitrates as precursors and ammonia water as the precipitator. A mixed metal nitrate solution was prepared with a total concentration of metals equal to 1 M. The nominal Cr/Al molar ratio was 1:1. The ammonia was added into the metal solution until $\text{pH} = 7.5$ under vigorous stirring and slight heating (50 °C). The reaction was carried out for 24 h. After reaction, precipitates were filtered, washed with distilled water, dried in a vacuum dryer below 0.10 atm at 200 °C for 16 h, and then calcined in air at 400 °C for 4 h. Prior to the XRD measurements, the samples were reduced in a stream of pure hydrogen at temperatures ranging from 400 to 1450 °C overnight. Then, the obtained samples were cooled in the flow of an inert gas to ambient temperature and sealed to avoid contact with the air.

2.2. Physicochemical Characterization

The phase transformation of the prepared mixture as a function of temperature was investigated by X-ray diffraction analysis. The diffraction patterns were collected using a PANalytical X'Pert Pro MPD diffractometer in Bragg Brentano reflection geometry (Malvern

Panalytical Ltd., Royston, UK). The diffractometer was equipped with a $\text{CuK}\alpha$ radiation source ($\lambda = 1.5418 \text{ \AA}$). Data were collected in the 2θ range of 5° – 80° with a step size of 0.0167° and exposure per step of 27 s.

For qualitative and Rietveld quantitative phase analyses, the PANalytical High Score software package (ver. 4.9) was used, combined with the International Centre for Diffraction Data's (ICDD) powder diffraction file (PDF-2 ver. 2020) database of standard reference materials. The structural details for Rietveld quantitative analyses were obtained from the Crystallography Open Database [23]. To estimate the full width at half maximum (FWHM) of the diffraction profiles, the pseudo-Voigt function was applied. Then, after taking into account the broadening caused by the diffractometer, the FWHM was used to calculate the size of the crystallites using the Scherrer equation.

$$D_{hkl} = \frac{K\lambda}{\beta_D \cos(\theta_{max})} \quad (1)$$

where $K = 0.9$, a dimensionless shape factor; λ is the wavelength of scattered X-ray radiation; β_D is the full width at half maximum of the hkl diffraction peak; and θ_{max} is the scattering angle at the maximum of the hkl diffraction peak. The unit cell parameters for CrAl_2O_4 were determined by the DICVOL04 algorithm [24].

2.3. Theoretical Calculations

In order to confirm the conjecture formulated on the basis of the experimental data, the proposed spinel structure of CrAl_2O_4 was optimized by computing the analytical gradients of the energy with respect to both unit cell parameters and atom coordinates, treating CrAl_2O_4 as a 3-dimensional crystal system. The calculations were performed using CRYSTAL17 [25,26] and we employed B3LYP density functional with D3 version of Grimme's dispersion [27]. The used basis set was the POB double- ζ polarization basis set (POB-DZVP) [28]. The initial structural parameters, which were taken as an input, were those found for the spinel structure of MgAl_2O_4 [29]. The data from the calculations were then compared with the experimental ones.

3. Results and Discussion

The formation of either separate aluminum and chromium oxides or their substitutional solution during the dehydration of corresponding hydroxides is governed mainly by the temperature of the process and the molar ratio of aluminum to chromium. According to the literature, at a temperature as high as 1250°C , these oxides can form $\text{Cr}_x\text{Al}_{2-x}\text{O}_3$ solid solution over a broad range of compositions ($0 \leq x \leq 2$). However, at a lower temperature, a miscibility gap is present, which originates from the different mechanisms of dehydration of aluminum and chromium hydroxides [30,31]. For instance, the dehydration of chromium hydroxide leads directly to the formation of $\alpha\text{-Cr}_2\text{O}_3$ at a temperature above 400°C , whereas the dehydration of aluminum hydroxide proceeds through the formation of aluminum oxyhydroxides, and then via different metastable alumina polymorphs, such as γ , δ , and θ , whose structure differs significantly from $\alpha\text{-Cr}_2\text{O}_3$. The formation of $\alpha\text{-Al}_2\text{O}_3$, which is isostructural with eskolaite, occurs only at a temperature above 1000°C [32].

The XRD measurements of the sample after calcination at 400°C revealed that the formed oxides are amorphous, as indicated by the absence of any diffraction peaks (Figure 1). At a higher reduction temperature (600°C), the weak broad diffraction maxima appeared at 2θ ca. 24.74° , 34.04° , 36.57° , and 55.53° , characteristic of the $\alpha\text{-Cr}_2\text{O}_3$ phase (JCPDS Card No. 01-082-3794).

This indicates that at this temperature, only chromium oxide started to crystallize, which is consistent with data reported in the literature [14]. The further increase in temperature up to 800°C resulted in an intensification and sharpening of those maxima as well as the appearance of new small diffraction peaks related to $\alpha\text{-Al}_2\text{O}_3$ phase (JCPDS Card No. 01-088-0826). Moreover, diffraction peaks of $\alpha\text{-Cr}_2\text{O}_3$ were slightly shifted toward a higher angle, indicating the formation of $(\text{Al,Cr})_2\text{O}_3$ substitution solution. The unit cell

parameters of the formed solid solution calculated from the peak (012) offset is presented in Table 1.

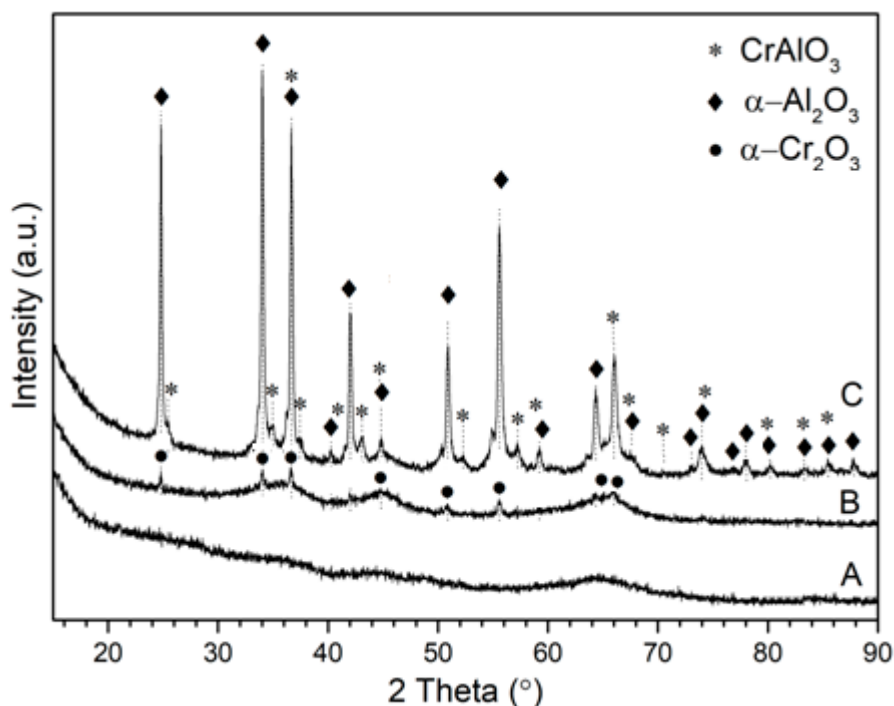


Figure 1. XRD patterns of the sample after calcination at 400 °C (A) and after subsequent reduction at 600 °C (B) and 800 °C (C).

Table 1. The unit cell parameters of (Al,Cr)₂O₃ and individual oxides.

Peak (012)	2θ (°)	a (Å)	c (Å)
Cr ₂ O ₃	24.732	4.960 (1)	13.598 (4)
(Al,Cr) ₂ O ₃ (~80% Cr ₂ O ₃)	24.786	4.900 (1)	13.435 (3)
α-Al ₂ O ₃	25.566	4.760 (1)	12.997 (3)

Based on a comparison with literature data [31], the content of Cr₂O₃ in solid solution was found to be ca. 80%. The formation of (Al,Cr)₂O₃ solid solution did not exclude the presence of isolated α-Cr₂O₃ phase, which is not detectable due to the overlap of diffraction peaks.

Notably, no other crystallographic phases of alumina were observed at this temperature. On the other hand, when the reduction process was performed at 1000 °C, the diffraction maxima of metastable alumina polymorphs appeared. Particularly, the characteristic diffraction peaks of γ-Al₂O₃ (JCPDS Card No. 01-074-4629) and χ-Al₂O₃ (JCPDS Card No. 00-051-0769) phases were observed at 31.66°, 36.91°, and 45.12°; and at 7.76°, 15.52°, and 33.42°, respectively (Figure 2). Such results imply that the formation of α-Al₂O₃ grains proceeds via two different pathways, depending on the initial location of their formerly amorphous form (Figure 3). The Al₂O₃ located in close proximity to chromium oxide tends to nucleate directly on its surface and then grow as α-Al₂O₃ (Figure 3, Route 2). The process can proceed at temperatures as low as 450 °C. On the contrary, the isolated grains of aluminum oxide crystallize as metastable forms, which then undergo structural transformation to thermodynamically stable α-Al₂O₃ (Figure 3, Route 1). The process is usually accomplished at temperatures above 1000 °C. The presence of both χ- and γ- may indicate that the dehydration process proceeds from different alumina precursors.

Particularly, it was reported that the γ is the first Al_2O_3 polymorph that is formed during the calcination/dehydration of boehmite, whereas χ - Al_2O_3 is initially formed from the gibbsite. Both hydroxides can be originally formed during the precipitation stage and/or as a result of decomposition of gibbsite to boehmite during calcination process. The formed $(\text{Al,Cr})_2\text{O}_3$ solution was not stable and decomposed under the investigated conditions, as evidenced by the disappearance of the corresponding diffraction maxima.

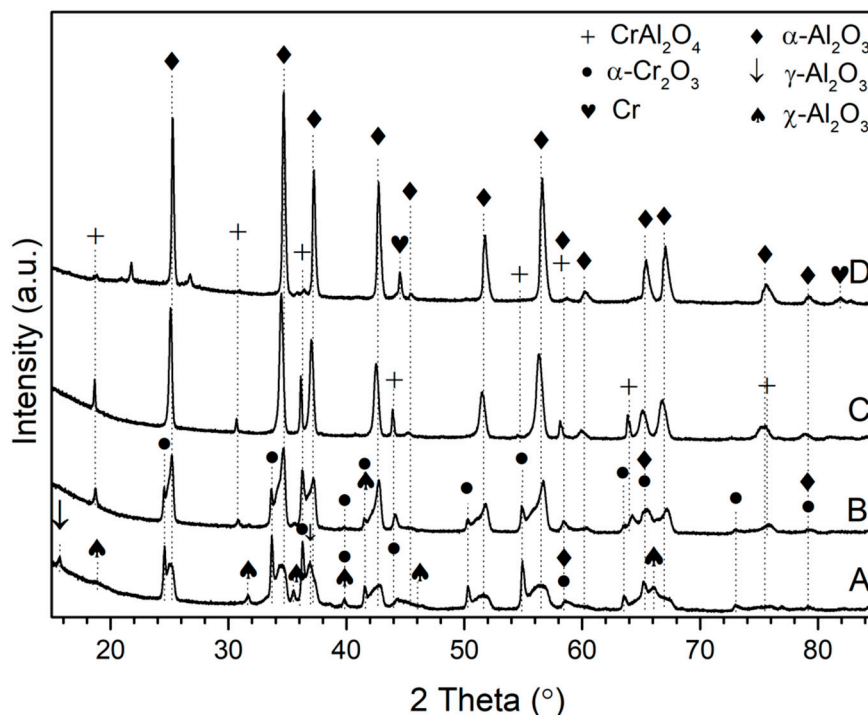


Figure 2. XRD patterns of the sample after reduction at 1000 (A), 1150 (B), 1300 (C), and 1450 (D) °C.

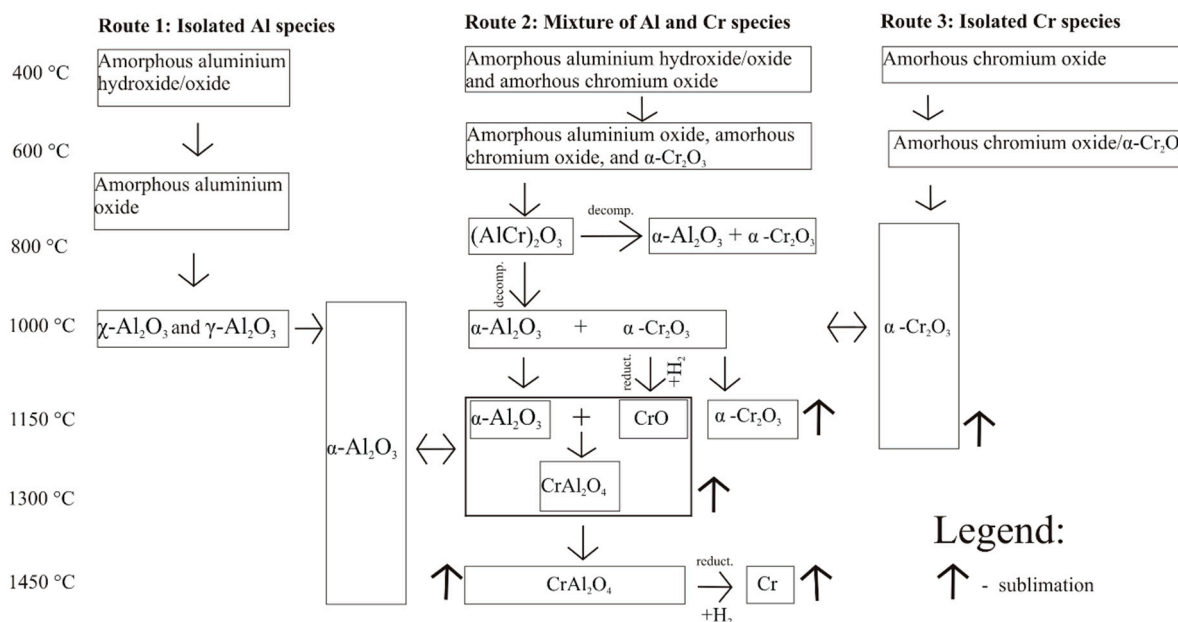


Figure 3. Phase transformation of co-precipitated Al and Cr oxides as a function of temperature.

At 1150 °C, the XRD measurements revealed the presence of diffraction peaks at 2θ ca. 18.68°, 30.79°, 36.29°, 44.35°, and 64.68°. A good matching of these peaks to the MgAl_2O_4

standard was noted (JCPDS Card No. 01-075-0713). In order to confirm the experimental data, theoretical calculations were performed. Assuming isostructurality with MgAl_2O_4 , good agreement between the experimental data and theoretical calculations was noted. On this basis, we think that a CrAl_2O_4 compound with a spinel structure can be formed. The ideal unit cell of the CrAl_2O_4 can be expressed as $\text{Cr}_8\text{Al}_{16}\text{O}_{32}$, in which 32 oxygen anions (occupying 48f positions), are face-centered cubic close packed with a space group Fd-3m, with eight CrAl_2O_4 units per cubic cell. The Cr^{2+} ions occupy tetrahedral 8a symmetry position between O^{2-} ions and the Al^{3+} ions are sited in octahedral 16d sites. To confirm the CrAl_2O_4 structure, we calculated the bond-valence parameters, as proposed by Gagné and Hawthorne [33], at the tetrahedrally and octahedrally coordinated sites. The bond valence sum at the four-fold site is 2.26 v.u., which is a little larger than the +2 expected for the Cr^{2+} cation; the bond valence sum at the six-fold site is 2.92 v.u., which is a little smaller than the +3 expected for the Al^{3+} cation. These bond valence values not only confirm that Cr^{2+} and Al^{3+} are the dominant cations at the tetrahedrally and octahedrally coordinated sites, respectively, but they also indicate the occurrence of a partial Cr-Al disorder (likely less than 10% in terms of Cr^{2+} content) over the tetrahedrally and octahedrally coordinated sites. This type of disorder is always present in Cr-bearing MgAl_2O_4 spinels [34]. Cámara et al. [35] reported occurrence of the mineral dellagiustaite, with ideal formula $\text{V}^{2+}\text{Al}_2\text{O}_4$, formed under super-reduced geological conditions from high-temperature melts trapped in corundum aggregates. Since dellagiustaite is an inverse spinel, the V^{2+} cations prefer six-fold coordination, unlike Cr^{2+} cations, which prefer four-fold coordination in our spinel structure. In our opinion, the spinel CrAl_2O_4 may be found in nature under very reducing conditions typical of basaltic systems [36]. However, no minerals containing Cr^{2+} have been reported so far [37]. In conclusion, to the best of our knowledge, the CrAl_2O_4 compound has not been described in the literature yet. Table 2 presents the comparison of the unit cell parameters and crystallographic data for the newly formed compound, calculated using the DICVOL04 procedure and the CRYSTAL17 package.

Table 2. Crystallographic analysis of CrAl_2O_4 (isostructural with MgAl_2O_4).

Crystal Data					
Experimental			Theoretical		
Crystal System	Space Group	a (Å)	Crystal System	Space Group	a (Å)
Cubic	Fd-3m	8.22 (3)	Cubic	Fd-3m	8.106 (2)
(hkl)	d_{hkl}		(hkl)	d_{hkl}	
(111)	4.75		(111)	4.680	
(022)	2.91		(022)	2.866	
(131)	2.48		(131)	2.444	
-	-		(222)	2.340	
(040)	2.16		(040)	2.206	
-	-		(133)	1.860	
-	-		(242)	1.655	
-	-		(151)	1.560	
(044)	1.45		(044)	1.433	
-	-		(153)	1.370	
-	-		(244)	1.351	

Please find the CIF and JPG file in Supplementary Materials.

On the basis of the obtained results, it can be postulated that at temperatures above 1150 °C, the $\alpha\text{-Cr}_2\text{O}_3$ undergoes reduction to CrO, the chromium ions of which further diffuse into an $\alpha\text{-Al}_2\text{O}_3$ matrix, forming CrAl_2O_4 . At further increasing temperatures, the agglomeration of the formed compounds was observed as evidenced by the increase in crystallite size of both spinel compound and alumina. Particularly, the size of the $\alpha\text{-}$

Al_2O_3 particle increased from 29 nm at 1150 °C to 54 nm at 1450 °C, whereas the size of the crystallites of CrAl_2O_4 increased from 27 nm at 1150 °C to 125 nm at 1300 °C. In general, the increase in temperature beyond 1000 °C resulted in a gradual decrease in chromium-containing compounds due to their sublimation (Table 3).

Table 3. Phase composition of the investigated samples during reduction at different temperatures.

Temperature, °C	Phase Composition	Crystallite Size, nm *	Relative Concentration, %
600	$\alpha\text{-Cr}_2\text{O}_3$	12	100
800	$\alpha\text{-Al}_2\text{O}_3$	~5	28
	CrAlO_3	50	72
1000	$\alpha\text{-Al}_2\text{O}_3$	15	45
	$\chi\text{-Al}_2\text{O}_3$	11	7
	$\gamma\text{-Al}_2\text{O}_3$	19	5
	$\alpha\text{-Cr}_2\text{O}_3$	49	43
1150	$\alpha\text{-Al}_2\text{O}_3$	29	55
	$\alpha\text{-Cr}_2\text{O}_3$	20	21
	CrAl_2O_4	27	24
1300	$\alpha\text{-Al}_2\text{O}_3$	40	85
	CrAl_2O_4	125	15
1450	$\alpha\text{-Al}_2\text{O}_3$	54	94
	CrAl_2O_4	25	3
	Cr	60	3

* The error in estimating the crystallite size is about 1–2 nm.

At 1450 °C, small residual amounts of metallic chromium were observed, which formed as a result of a reduction of the spinel compound. All attempts to obtain pure CrAl_2O_4 spinel in order to study its physical properties more closely have failed. When exposed to ambient conditions, the Cr–Al spinel structure is metastable and readily undergoes oxidation to individual oxides. The general scheme of phase transformation of co-precipitated oxides as a function of temperature is depicted in Figure 3.

4. Summary

The obtained results showed that the crystallization of atomically mixed amorphous Al–Cr oxides proceeds first via the formation of $\alpha\text{-Cr}_2\text{O}_3$, followed by the nucleation and growth of $\alpha\text{-Al}_2\text{O}_3$ on its surface. Isolated grains of Al_2O_3 are also present as indicated by the crystallization of metastable alumina phases, which are subsequently converted into $\alpha\text{-Al}_2\text{O}_3$ at high temperature. Under harsh reductive conditions, the investigated oxides are partially transformed to Cr–Al spinel compound. It is proposed that the formation of this structure is due to the formation of Cr^{2+} ions (because of reduction of $\alpha\text{-Cr}_2\text{O}_3$) and then interdiffusion of Al^{3+} and Cr^{2+} ions through the oxygen array.

Supplementary Materials: The following are available online at <https://www.mdpi.com/article/10.3390/ma14123218/s1>. CIF and JPG file of the CrAl_2O_4 compound.

Author Contributions: Conceptualization, O.S. and T.M.; Software, T.S.; Investigation, W.M., R.C., A.K., V.S., T.S.; Writing–Original Draft Preparation, O.S.; Writing–Review & Editing, W.M. All authors have read and agreed to the published version of the manuscript.

Funding: This research received no external funding.

Institutional Review Board Statement: Not applicable.

Informed Consent Statement: Not applicable.

Data Availability Statement: The data presented in this study are available on request from the corresponding author.

Acknowledgments: The calculations mentioned in this paper were performed using TUL Computing & Information Services Center infrastructure.

Conflicts of Interest: The authors declare no conflict of interest.

References

1. Shirai, T.; Watanabe, H.; Fuji, M.; Takahashi, M. Structural Properties and Surface Characteristics on Aluminum Oxide Powders. *Annu. Rep. Adv. Ceram. Res. Cent. Nagoya Inst. Technol.* **2009**, *9*, 23–31.
2. Abyzov, A.M. Aluminum Oxide and Alumina Ceramics (review). Part 1. Properties of Al₂O₃ and Commercial Production of Dispersed Al₂O₃. *Refract. Ind. Ceram.* **2019**, *60*, 24–32. [[CrossRef](#)]
3. Trueba, M.; Trasatti, S.P. γ -alumina as a support for catalysts: A review of fundamental aspects. *Eur. J. Inorg. Chem.* **2005**, *2005*, 3393–3403. [[CrossRef](#)]
4. Chu, T.P.M.; Nguyen, N.T.; Vu, T.L.; Dao, T.H.; Dinh, L.C.; Nguyen, H.L.; Hoang, T.H.; Le, T.S.; Pham, T.D. Synthesis, characterization, and modification of alumina nanoparticles for cationic dye removal. *Materials* **2019**, *12*, 450. [[CrossRef](#)]
5. Wang, Z.; Wu, W.; Bian, X.; Wu, Y. Synthesis and characterization of amorphous Al₂O₃ and γ -Al₂O₃ by spray pyrolysis. *Green Process. Synth.* **2016**, *5*, 305–310. [[CrossRef](#)]
6. Digne, M.; Sautet, P.; Raybaud, P.; Toulhoat, H.; Artacho, E. Structure and stability of aluminum hydroxides: A theoretical study. *J. Phys. Chem. B* **2002**, *106*, 5155–5162. [[CrossRef](#)]
7. Karabulut, Ş.; Gökmen, U.; Çinici, H. Study on the mechanical and drilling properties of AA7039 composites reinforced with Al₂O₃/B₄C/SiC particles. *Compos. Part B Eng.* **2016**, *93*, 43–55. [[CrossRef](#)]
8. Yang, K.; Zhou, X.; Zhao, H.; Tao, S. Microstructure and mechanical properties of Al₂O₃-Cr₂O₃ composite coatings produced by atmospheric plasma spraying. *Surf. Coat. Technol.* **2011**, *206*, 1362–1371. [[CrossRef](#)]
9. Cai, K.F.; McLachlan, D.S.; Axen, N.; Manyatsa, R. Preparation, microstructures and properties of Al₂O₃-TiC composites. *Ceram. Int.* **2002**, *28*, 217–222. [[CrossRef](#)]
10. Tuan, W.H.; Chen, R.Z.; Wang, T.C.; Cheng, C.H.; Kuo, P.S. Mechanical properties of Al₂O₃/ZrO₂ composites. *J. Eur. Ceram. Soc.* **2002**, *22*, 2827–2833. [[CrossRef](#)]
11. Hirata, T.; Morimoto, T.; Deguchi, A.; Uchida, N. Corrosion resistance of alumina-chromia ceramic materials against molten slag. *Mater. Trans.* **2002**, *43*, 2561–2567. [[CrossRef](#)]
12. Kafkaslıoğlu Yıldız, B.; Yılmaz, H.; Tür, Y.K. Evaluation of mechanical properties of Al₂O₃-Cr₂O₃ ceramic system prepared in different Cr₂O₃ ratios for ceramic armour components. *Ceram. Int.* **2019**, *45*, 20575–20582. [[CrossRef](#)]
13. Kim, K.J.; Chang, C.H.; Ahn, H.G. The effect of zinc oxide addition to alumina-supported gold catalyst in low temperature carbon monoxide oxidation. *J. Nanosci. Nanotechnol.* **2015**, *15*, 660–664. [[CrossRef](#)]
14. Eklund, P.; Sridharan, M.; Sillassen, M.; Böttiger, J. α -Cr₂O₃ template-texture effect on α -Al₂O₃ thin-film growth. *Thin Solid Films* **2008**, *516*, 7447–7450. [[CrossRef](#)]
15. Bosi, F.; Hatert, F.; Hålenius, U.; Pasero, M.; Miyawaki, R.; Mills, S.J. On the application of the IMA–CNMNC dominant-valency rule to complex mineral compositions. *Mineral. Mag.* **2019**, *83*, 627–632. [[CrossRef](#)]
16. Zhao, P.; Zhao, H.; Yu, J.; Zhang, H.; Gao, H.; Chen, Q. Crystal structure and properties of Al₂O₃-Cr₂O₃ solid solutions with different Cr₂O₃ contents. *Ceram. Int.* **2018**, *44*, 1356–1361. [[CrossRef](#)]
17. Sako, E.Y.; Braulio, M.A.L.; Zinngrebe, E.; Van Der Laan, S.R.; Pandolfelli, V.C. Fundamentals and applications on in situ spinel formation mechanisms in Al₂O₃-MgO refractory castables. *Ceram. Int.* **2012**, *38*, 2243–2251. [[CrossRef](#)]
18. Ping, L.R.; Azad, A.M.; Dung, T.W. Magnesium aluminate (MgAl₂O₄) spinel produced via self-heat-sustained (SHS) technique. *Mater. Res. Bull.* **2001**, *36*, 1417–1430. [[CrossRef](#)]
19. Bosi, F.; Biagioni, C.; Pasero, M. Nomenclature and classification of the spinel supergroup. *Eur. J. Mineral.* **2019**, *31*, 183–192. [[CrossRef](#)]
20. Rossi, R.C.; Fulrath, R.M. Epitaxial Growth of Spinel by Reaction in the Solid State. *J. Am. Ceram. Soc.* **1963**, *46*, 145–149. [[CrossRef](#)]
21. CARTER, R.E. Mechanism of Solid-state Reaction Between Magnesium Oxide and Aluminum Oxide and Between Magnesium Oxide and Ferric Oxide. *J. Am. Ceram. Soc.* **1961**, *44*, 116–120. [[CrossRef](#)]
22. NAVIAS, L. Preparation and Properties of Spinel Made by Vapor Transport and Diffusion in the System MgO-Al₂O₃. *J. Am. Ceram. Soc.* **1961**, *44*, 434–446. [[CrossRef](#)]
23. Quirós, M.; Gražulis, S.; Girdzijauskaitė, S.; Merkys, A.; Vaitkus, A. Using SMILES strings for the description of chemical connectivity in the Crystallography Open Database. *J. Cheminform.* **2018**, *10*, 1–17. [[CrossRef](#)] [[PubMed](#)]
24. Boultif, A.; Louer, D. Indexing of powder diffraction patterns for low-symmetry lattices by the successive dichotomy method. *J. Appl. Crystallogr.* **1991**, *24*, 987–993. [[CrossRef](#)]
25. Dovesi, R.; Erba, A.; Orlando, R.; Zicovich-Wilson, C.M.; Civalleri, B.; Maschio, L.; Rérat, M.; Casassa, S.; Baima, J.; Salustro, S.; et al. Quantum-mechanical condensed matter simulations with CRYSTAL. *Wiley Interdiscip. Rev. Comput. Mol. Sci.* **2018**, *8*, e1360. [[CrossRef](#)]

26. Dovesi, R.; Saunders, V.R.; Roetti, C.; Orlando, R.; Zicovich-Wilson, C.M.; Pascale, F.; Civalieri, B.; Doll, K.; Harrison, N.M.; Bush, I.J.; et al. *CRYSTAL 14: User's Manual*; University of Turin; Turin, Italy, 2016; pp. 1–382.
27. Grimme, S.; Antony, J.; Ehrlich, S.; Krieg, H. A consistent and accurate ab initio parametrization of density functional dispersion correction (DFT-D) for the 94 elements H-Pu. *J. Chem. Phys.* **2010**, *132*, 154104. [[CrossRef](#)]
28. Vilela Oliveira, D.; Laun, J.; Peintinger, M.F.; Bredow, T. BSSE-correction scheme for consistent gaussian basis sets of double—and triple-zeta valence with polarization quality for solid-state calculations. *J. Comput. Chem.* **2019**, *39*, 1285–1290. [[CrossRef](#)]
29. Kvitka, N.G.; Zorina, S.S. Refinement of the structure of the spinel Al_2MgO_4 . *Sov. Phys. Crystallogr.* **1969**, *13*, 599–600.
30. Edlmayr, V.; Pohler, M.; Letofsky-Papst, I.; Mitterer, C. Microstructure and thermal stability of corundum-type $(\text{Al}_{0.5}\text{Cr}_{0.5})_2\text{O}_3$ solid solution coatings grown by cathodic arc evaporation. *Thin Solid Films* **2013**, *534*, 373–379. [[CrossRef](#)]
31. Bondioli, F.; Ferrari, A.M.; Leonelli, C.; Manfredini, T.; Linati, L. Reaction Mechanism in Alumina/Chromia (Al_2O_3 – Cr_2O_3) Solid Solutions Obtained by Coprecipitation. *J. Am. Ceram. Soc.* **2000**, *83*, 2036–2040. [[CrossRef](#)]
32. Mahat, A.M.; Mastuli, M.S.; Kamarulzaman, N. Influence of annealing temperature on the phase transformation of Al_2O_3 . *AIP Conf. Proc.* **2016**, *1711*, 050001. [[CrossRef](#)]
33. Gagné, O.C.; Hawthorne, F.C. Comprehensive derivation of bond-valence parameters for ion pairs involving oxygen. *Acta Crystallogr. Sect. B Struct. Sci. Cryst. Eng. Mater.* **2015**, *71*, 562–578. [[CrossRef](#)]
34. Bosi, F.; Andreozzi, G.B. Chromium influence on Mg-Al intracrystalline exchange in spinels and geothermometric implications. *Am. Mineral.* **2017**, *102*, 333–340. [[CrossRef](#)]
35. Cámara, F.; Bindi, L.; Pagano, A.; Pagano, R.; Gain, S.E.M.; Griffin, W.L. Dellagiustaita: A novel natural spinel containing V^{2+} . *Minerals* **2019**, *9*, 4. [[CrossRef](#)]
36. Hanson, B.; Jones, J.H. The systematics of Cr^{3+} and Cr^{2+} partitioning between olivine and liquid in the presence of spinel. *Am. Mineral.* **1998**, *83*, 669–684. [[CrossRef](#)]
37. Liu, C.; Hystad, G.; Golden, J.J.; Hummer, D.R.; Downs, R.T.; Morrison, S.M.; Ralph, J.P.; Hazen, R.M. Chromium mineral ecology. *Am. Mineral.* **2017**, *102*, 612–619. [[CrossRef](#)]